Acta Materialia 112 (2016) 132–140

Contents lists available at ScienceDirect

Acta Materialia

journal homepage: www.elsevier.com/locate/actamat

Full length article

Flow-induced elastic anisotropy of metallic glasses

Y.H. Sun [a], A. Concustell [b], M.A. Carpenter [c], J.C. Qiao [d], A.W. Rayment [a], A.L. Greer [a, *]

[a] Department of Materials Science and Metallurgy, University of Cambridge, 27 Charles Babbage Road, Cambridge CB3 0FS, UK
[b] Department of Materials Science and Metallurgical Engineering, University of Barcelona, Spain
[c] Department of Earth Sciences, University of Cambridge, UK
[d] School of Mechanics & Civil Architecture, Northwestern Polytechnical University, Shaanxi, China

ARTICLE INFO

Article history:
Received 28 February 2016
Received in revised form
6 April 2016
Accepted 7 April 2016
Available online 18 April 2016

Keywords:
Metallic glass
Anisotropy
Elastic properties
Non-Newtonian flow
Anelasticity

ABSTRACT

As-cast bulk metallic glasses are isotropic, but anisotropy can be induced by thermomechanical treatments. For example, the diffraction halo in the structure function $S(Q)$ observed in transmission becomes elliptical (rather than circular) after creep in uniaxial tension or compression. Published studies associate this with frozen-in anelastic strain and bond-orientational anisotropy. Results so far are inconsistent on whether viscoplastic flow of metallic glasses can induce anisotropy. Preliminary diffraction data suggest that the anisotropy, if any, is very low, while measurements of the elastic properties suggest that there is induced anisotropy, opposite in sign to that due to anelastic strain. We study three bulk metallic glasses, $Ce_{65}Al_{10}Cu_{20}Co_5$, $La_{55}Ni_{10}Al_{35}$, and $Pd_{40}Ni_{30}Cu_{10}P_{20}$. By using resonant ultrasound spectroscopy to determine the full elasticity tensor, the effects of relaxation and rejuvenation can be reliably separated from uniaxial anisotropy (of either sign). The effects of viscoplastic flow in tension are reported for the first time. We find that viscoplastic flow of bulk metallic glasses, particularly in tension, can induce significant anisotropy that is distinct from that associated with frozen-in anelastic strain. The conditions for inducing such anisotropy are explored in terms of the Weissenberg number (ratio of relaxation times for primary relaxation and for shear strain rate). There is a clear need for further work to characterize the structural origins of flow-induced anisotropy and to explore the prospects for improved mechanical and other properties through induced anisotropy.

1. Introduction

A glass is commonly expected to be isotropic, but can be anisotropic, even when formed from a liquid composed of atoms or of molecules that are not orientable. Early studies of metallic glasses were on ribbons produced by melt-spinning, a directional process that involves strong shearing of the liquid cooling into the glassy state [1]. Evidence of anisotropy soon emerged: the ribbons densify on annealing, but the contraction strain parallel to the length is about twice that parallel to the width [2,3]. Small-angle neutron scattering suggests aligned defects possibly connected with the shearing [4,5]. Both X-ray and neutron scattering show that the structure function $S(Q)$ is different in different directions in ribbons [6,7]. The yield stress has been measured in tension parallel to the ribbon length and parallel to the width; it is consistently higher parallel to the length, typically by a few percent but possibly by much more [8,9]. Resonant ultrasound spectroscopy (RUS) suggests that the ribbon elasticity is (within ~3%) isotropic in plane, but that the stiffness coefficient C_{33} normal to the ribbon is much greater than the coefficients C_{11} and C_{22} in the plane [10]. This greater difference normal to the ribbon is consistent with structural studies [7]. In deposited thin films, there are substrate and stress effects that complicate the interpretation of measured properties. Nevertheless, intrinsic structural anisotropy can be expected from the directionality of growth and the symmetry-breaking nature of surface mobility, as analysed for amorphous metallic deposits [11], and also seen in organic ultrastable glasses [12]. In contrast with ribbons and thin films, bulk metallic glasses (BMGs) are expected to be much closer to isotropy in their as-cast state, and this has been confirmed by RUS measurement of the full elasticity tensor [13].

Melt-spun ribbons and thin films show that metallic glasses can be significantly anisotropic. The present work explores whether similar or even greater degrees of anisotropy can be induced in BMGs. This may be of practical interest in optimizing properties (within the general field of thermomechanical processing to access new glassy states [14]), and of fundamental interest in probing the

* Corresponding author.
E-mail address: alg13@cam.ac.uk (A.L. Greer).

http://dx.doi.org/10.1016/j.actamat.2016.04.022

mechanisms of flow and plasticity. In BMG samples under applied stress, anisotropic elastic strains can be detected in diffraction studies [15]. Subsequent work of similar kind (reviewed in Ref. [16]) has included loading into the plastic regime in which there is inhomogeneous flow (sharply localized in *shear bands* [17]). In this regime, however, diffraction studies may no longer provide a quantitative measure of elastic strains [18].

In the present work, in contrast, our focus is on structural changes in unstressed BMG samples as a result of prior mechanical treatment, in particular homogeneous viscoplastic flow associated with creep under uniaxial load. For such samples, X-ray diffraction patterns obtained in transmission, using a synchrotron source, show a circular first halo for isotropic as-cast BMGs. Under load, or in the stress-free state after creep, this halo is elliptical, the first halo in $S(Q)$ occurring at lower Q in the direction of positive (tensile) strain, and vice versa [19].

On loading a metallic glass below the macroscopic yield stress, there are three contributions to the strain [20]: elastic ε_e (instantaneous and recoverable), anelastic ε_a (time-dependent, recoverable), and viscoplastic ε_v (time-dependent, non-recoverable). In the early stages of creep, the induced anisotropy is clearly associated with ε_a, and is removed on subsequent stress-free annealing [21]. The degree of anisotropy (measured in stress-free samples after homogeneous creep deformation) can be quantified as the relative difference $\Delta Q/Q$ in the major and minor axes of the first-halo ellipse in the diffraction pattern in transmission. In the early stages dominated by ε_a, the induced anisotropy ($\Delta Q/Q$) in a BMG is typically 5–10% [22]. In later stages, for example with total creep strains $(\varepsilon_a + \varepsilon_v) > 30\%$, the resulting samples have very low diffraction anisotropy ($\Delta Q/Q \approx 0.3\%$), and the anisotropy decreases with further elongation, particularly for strains >60% [23].

Anelasticity can be associated with the activation of shear transformation zones (STZs) under load. Directional operation of the STZs (in tension, this involves bond-breaking parallel to the tensile axis and bond-forming perpendicular to the axis [6]) allows them to deform in response to the load, but they are embedded in a comparatively rigid matrix. After unloading, the elastic strain in the matrix contributes to the observed diffraction anisotropy and also provides the driving force for anelastic recovery. At large creep strains, the activation of many STZs destroys the memory inherent in the matrix, and consequently ε_a and the measured anisotropy decrease. The strain that gives the ellipticity of the first diffraction halo is associated with bond-orientational anisotropy [6,20,24]. In this picture, induced anisotropy arises only from anelastic deformation; at larger strains associated with viscoplastic flow, there may be little or no induced anisotropy. This would be consistent with the lack of anisotropy in a liquid undergoing Newtonian flow (i.e. with viscosity, and presumably structure, independent of shear rate), but further examination is required for non-Newtonian flow of a glass or liquid.

The soft-magnetic properties of metallic glasses are the basis of their principal applications. From the many studies of magnetic properties, we consider magnetic anisotropy induced by creep. Nielsen et al. have shown that in (Co,Fe)-based metallic-glass ribbons subjected to tensile creep, there are two opposing contributions to induced anisotropy. One is recoverable and associated with ε_a; the other, of opposite sign, is non-recoverable and associated with ε_v [25–27]. Although magnetoelastic interactions must be relevant, both these contributions are non-zero even in glass compositions showing zero magnetostriction [26]. The anelastic contribution to anisotropy is clearly stronger than that from viscoplastic flow [26], and some have claimed that the latter is negligible, with all the induced anisotropy being recoverable [28,29]. In this context, it is interesting that RUS measurements [13] of the full elasticity tensor of a BMG subjected to uniaxial compression show clear evidence of two opposing contributions to anisotropy from ε_a and ε_v; furthermore, at high enough strains (>~–20%), the latter (non-recoverable) contribution can be greater.

That work, on $Pd_{40}Cu_{30}Ni_{10}P_{20}$ BMG [13], is extended to other compositions in the present work, which also examines the role of tensile as well as compressive creep. It is well accepted that frozen-in anelastic strain in metallic glasses is associated with, and indeed must lead to, anisotropy in structure and properties. The present work instead focuses on the more disputed role of viscoplastic flow: there is no currently accepted model for how this can induce anisotropy in metallic glasses. There are, however, suggestions, for example from measurements of giant magnetoimpedance [30], that viscoplastic flow can induce significant anisotropy. We use elasticity measurements to provide a quantifiable comparison with the effects of anelastic strain: what is the extent of anisotropy that can be induced by viscoplastic flow, and what are the underlying mechanisms? While anisotropy in metallic glasses is important in magnetic properties, its role in optimizing mechanical properties remains largely unexplored, apart from preliminary studies [31]. There may be opportunities: we note that good mechanical properties, for example in high-performance fibres, can be based on aligned anisotropic structures.

2. Experimental methods

Metallic glasses with compositions (at.%) $Pd_{40}Cu_{30}Ni_{10}P_{20}$, $La_{55}Ni_{10}Al_{35}$ and $Ce_{65}Al_{10}Cu_{20}Co_5$ were studied. Rods, 3 mm in diameter and 70–80 mm in length, were prepared by suction-casting, and their glassy nature was confirmed by X-ray diffraction (D8 DaVinci, Bruker, CuKα radiation) (Fig. 1a). Differential scanning calorimetry (Q2000, TA Instruments), at a heating rate of 20 K min^{-1}, was used to determine the glass-transition temperature, T_g (Fig. 1b): the values are 569 K (Pd-based), 473 K (La-based) and 373 K (Ce-based). The Pd-based composition permits comparison with previous work [13]; it is resistant to crystallization and oxidation. The Ce-based composition is distinctly more machinable than Pd-based; it is chosen to permit preparation of 'dog-bone' samples for tensile tests. The La-based composition with intermediate T_g facilitates quenching in the effects of high-temperature treatments.

Uniaxial mechanical tests (H25K-S UTM, Tinius Olsen) were conducted at room temperature (RT) and at elevated temperature. Two type-K thermocouples were spot-welded to the upper and lower silicon-nitride anvils. The lower-anvil thermocouple provided the input to a Eurotherm temperature-controller. Heating was by an infrared emitter (Omega, Heraeus) 79 mm in diameter with 180° gold reflector, allowing rapid contact-free heating of the sample to the test temperature. The position of the infrared emitter was adjusted to ensure that both anvils reached the same temperature. The set temperature was reached in few minutes, but it took longer to establish full stability: 10–15 min in the smaller chamber used for compression tests and 40 min for the larger chamber used for tensile tests. The applied load was maintained at zero to avoid any creep during pre-test stabilization.

For compression tests, cylindrical samples with a height-to-diameter ratio of 1.7 (Pd-based) or 2.0 (La- & Ce-based) were cut from the cast rods. The end-faces were polished to make sure they are parallel to each other and perpendicular to the rod axis. The samples were placed on the bottom anvil, surrounded by the infrared emitter and then contacted by the upper anvil. Lubricant (copper paste) was used on the end surfaces to reduce barrelling of the sample in compression. After a steady, uniform temperature was attained, each test was conducted up to a given strain; the heating was then stopped and the load removed. The sample was removed from the mechanical testing machine, and quenched in

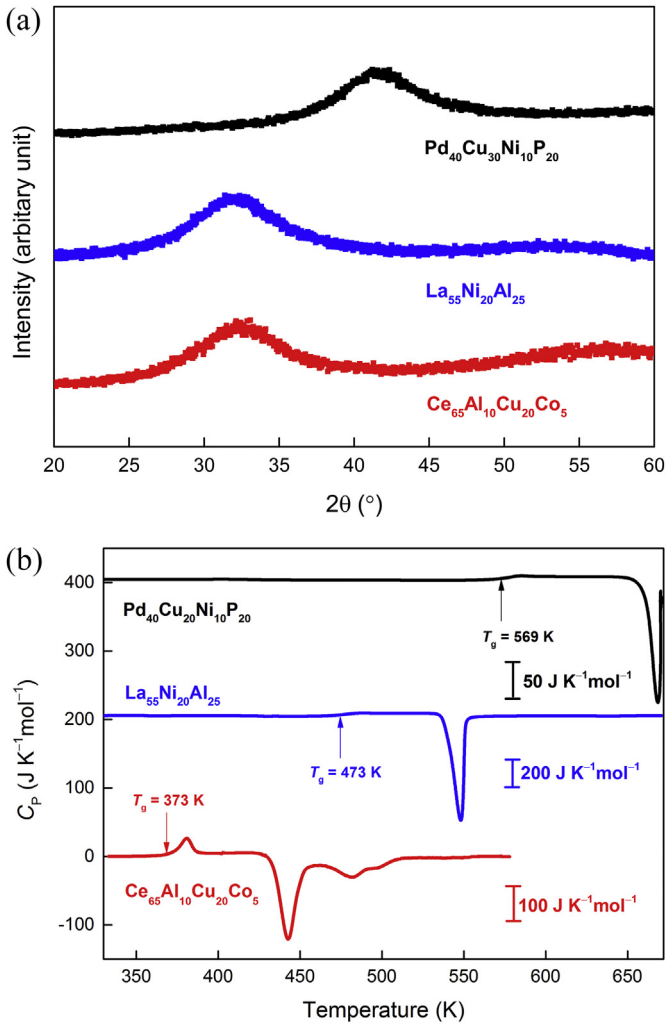

Fig. 1. Characterization of as-cast samples of the three BMGs studied in the present work: (a) X-ray (CuKα) diffraction traces (Bragg-Brentano geometry) showing that the samples are without any obvious crystallinity; (b) differential scanning calorimetry traces (heating at 20 K min^{-1}; downward deflection is exothermic), showing the step increase in specific heat capacity at the glass-transition temperature T_g (arrowed) in each alloy.

water (for Pd-based) or liquid nitrogen (for La- and Ce-based). The thin oxide layer that developed on the samples was easily removed by further polishing.

For tension tests, 3-mm-diameter rods of the Ce-based BMG were machined into a dog-bone shape with a gauge section 2 mm in diameter and 14 mm long. After the test, the sample was removed and quenched into liquid nitrogen.

Two types of loading were used. The results of tests under constant load (creep tests) are collected in Table 1. The results of tests under constant displacement rate (giving a constant engineering-strain rate) are collected in Table 2.

Measurements of the elasticity tensor were carried out with resonant ultrasound spectroscopy (RUS), using the apparatus and methods as in McKnight et al. [32,33]. Accurate alignment during deformation, and accurate sample shape after deformation, are essential to obtain a useful RUS spectrum. All deformation treatments were carried out on cylindrical samples. In most of the work, RUS measurements were made on cuboids with typical dimensions 1.5 × 2.0 × 3.5 mm, cut and polished from the deformed cylinders. The angles between the faces of the cuboids were checked under an optical microscope to ensure that they were within the range 90.0 ± 0.5°. In the case of the work on relaxation and rejuvenation (on the La-based BMG, Section 3.1), the as-cast cylindrical sample retained its shape after annealing and creep at RT; RUS measurements were made on the sample without further preparation. After the final treatment of this sample, creep at 380 K, a cuboid was cut from the deformed cylinder for the RUS measurement.

For each RUS sample, a resonance spectrum was collected, typically in the range 0.25–2.0 MHz with 6.5 × 10^5 data points. Frequencies were determined for the first 25–40 resonance peaks. The free vibration modes depend on the sample dimensions and the material density and stiffness coefficients (C_{ij}). Linear dimensions were measured using a micrometer to an accuracy of ±1 μm. The masses of samples were determined to an accuracy of ±0.1 mg. For a cuboid sample, the uncertainty in the density calculated from the mass and dimensions is dominated by the uncertainty in the mass, and is approximately ±0.3%. For cylindrical samples, because of their larger mass, the uncertainty in density is less, ±0.1%. While the uncertainty in density affects the calculated modulus values, it does not affect the accuracy of A (modulus ratio).

Thermomechanical treatments of metallic glasses cause changes in density. The largest change observed in the present work is a 0.22% increase on annealing the La-based BMG annealed at 380 K for 6 days. In principle, it would be desirable to determine the density independently for each sample after treatment. Given the error in density measurement, however, it is preferable to use the original cylinder density in the calculations of elastic properties. Density changes are associated with dimension changes, each affecting the measured resonance frequencies. An error in density of x% (due to a treatment that gives a change in density that is not taken into account) would give an error in calculated modulus of (x/3)%. For typical density changes, use of the original cylinder density thus leads to errors in the calculated modulus values of up to approximately ±0.05%.

Given the density and dimensions, the values of C_{ij} were determined by iteration, matching observed resonances with frequencies calculated using DRS software [34]. The resonant frequencies were fitted, taking the material to be transverse-isotropic (TI). With reference axes as in Fig. 2, isotropy is expected in the 1,2 plane. There are five independent coefficients: C_{11}, C_{12}, C_{13}, C_{33}, C_{44}; $C_{66} = (C_{11}-C_{12})/2$. The root-mean-square (rms) errors in the fitted values of the peak frequencies are 0.5% or less, representing a very good fit [35] (Tables 1 and 2). The calculated values of the stiffness coefficients, however, show a range of rms uncertainties: C_{11} (±0.5%), C_{33} (±0.5%), C_{12} (±0.8%), C_{13} (±1.2%), C_{44} (±0.15%), C_{66} (±0.15%). To characterize the samples, we choose the coefficients with the lowest uncertainties: these are the modulus $C_{44} \equiv G_4$ (for shear in planes parallel to the loading axis) and the modulus $C_{66} \equiv G_6$ (for shear in the transverse plane of the sample). For isotropy $C_{44} = C_{66}$, and we quantify the anisotropy A (Tables 1 and 2) as:

$$A = (G_4 - G_6)/G_4. \quad (1)$$

Values of A, a ratio of moduli, are of course not affected by any errors arising from changes in sample density.

3. Results

3.1. Relaxation and rejuvenation

The $La_{55}Ni_{10}Al_{35}$ BMG was used to explore the range of effects of thermomechanical treatments on elastic properties. To facilitate comparison of different states of the glass when the property changes might be slight, all measurements were made on a single

Table 1
Constant-load (creep) tests on $La_{55}Ni_{20}Al_{25}$ and $Ce_{65}Al_{10}Cu_{20}Co_5$ metallic glasses in uniaxial compression. Data on as-cast and stress-free annealed samples are given for comparison. The shear moduli G_4 and G_6 are determined by RUS on cylindrical or cuboid samples. With axes as in Fig. 2, G_4 applies when either the shear direction or shear-plane normal is parallel to the axis of the rod; G_6 applies when the shear direction and shear-plane normal both lie in the transverse plane. The low rms errors in the modulus values indicate that good fittings to the RUS data are obtained by assuming that the samples are transverse-isotropic. The anisotropy A is defined as $(G_4-G_6)/G_4$.

Sample treatment	Conditions	σ (MPa)	σ/σ_y	rms error (%)	G_4 (GPa)	G_6 (GPa)	A (%)
$La_{55}Ni_{20}Al_{25}$							
As-cast	RT = 300 K	0	0	0.49	15.29	15.25	+0.26
Annealed (1 day)	T_{anneal} = 380 K	0	0	0.46	15.63	15.61	+0.13
Annealed (6 day)	T_{anneal} = 380 K	0	0	0.50	15.77	15.80	−0.19
Crept (1 day)	T_{creep} = 300 K	200	0.3	0.45	15.73	15.74	−0.06
Crept (2 h)	T_{creep} = 380 K	200	0.3	0.42	15.56	15.77	−1.3
$Ce_{65}Al_{10}Cu_{20}Co_5$							
As-cast	RT = 300 K	0	0	0.40	12.00	11.95	+0.41
Crept (40 min)	T_{creep} = 333 K	150	0.3	0.39	11.98	11.83	+1.3

Table 2
Constant-shear-rate tests on $Pd_{40}Cu_{30}Ni_{10}P_{20}$ and $Ce_{65}Al_{10}Cu_{20}Co_5$ metallic glasses in uniaxial compression (C) or tension (T). The shear moduli G_4 and G_6 and the induced anisotropy A are as defined in Table 1. The values given are for engineering-strain rate, obtained from tests conducted at constant cross-head displacement rate.

Strain regime	T (K)	T/T_g	$\log(\dot{\varepsilon})(s^{-1})$	Final strain (%)	rms error (%)	G_4 (GPa)	G_6 (GPa)	A (%)
$Pd_{40}Cu_{30}Ni_{10}P_{20}$								
anelastic (C)	548	0.963	−3	0.8	0.24	34.08	34.30	−0.65
viscoplastic (C)	548	0.963	−3	6	0.35	34.07	34.05	+0.06
viscoplastic (C)	548	0.963	−3	13	0.39	34.27	34.00	+0.80
viscoplastic (C)	548	0.963	−3	33	0.25	34.97	34.11	+2.5
anelastic (C)	552	0.970	−2	0.8	0.34	34.07	34.74	−1.9
viscoplastic (C)	552	0.970	−2	13	0.38	34.93	34.47	+1.3
viscoplastic (C)	552	0.970	−2	37	0.32	34.39	33.87	+1.6
viscoplastic (C)	569	1.000	−3	33	0.42	34.37	34.42	−0.15
$Ce_{65}Al_{10}Cu_{20}Co_5$								
elastic (C)	298	0.798	−4	1.8[a]	*no*	broken		
elastic (C)	298	0.798	−4	2.1[a]	*no*	broken		
elastic (C)	298	0.798	−4	1.9[a]	*no*	broken		
elastic (C)	343	0.920	−3	1.8[a]	*no*	broken		
elastic (C)	378	1.013	−1	1.6[a]	*no*	broken		
viscoplastic (C)	343	0.920	−4	40	0.32	11.71	11.63	+0.69
viscoplastic (C)	353	0.946	−3	40	0.21	11.81	11.77	+0.34
viscoplastic (C)	363	0.973	−3	40	0.34	11.80	11.84	−0.31
viscoplastic (C)	373	1.000	−3	40	0.34	11.86	11.83	+0.25
viscoplastic (C)	383	1.027	−3	40	0.28	12.02	12.00	+0.18
viscoplastic (C)	363	0.973	−2	40	0.28	11.92	11.68	+2.0
viscoplastic (T)	368	0.987	−2	27[b]	0.33	12.16	12.72	−4.4
viscoplastic (T)	368	0.987	−2	27[b]	0.33	12.30	12.94	−5.0

[a] Calculated from peak stress divided by Young's modulus.
[b] Calculated from reduction of cross-section area in the uniform gauge section.

sample. After each treatment, RUS was used to determine the shear moduli G_4 and G_6. The results are shown in Table 1, and in Fig. 3, where the shaded band represents isotropy ($G_4 = G_6$) within the experimental uncertainties in the modulus values (±0.02 GPa) from the RUS fitting.

The as-cast sample is slightly anisotropic ($A = +0.26\%$), but the data point overlaps the shaded band. The sample is then annealed at 380 ± 2 K (0.8 T_g) for 24 h, inducing structural relaxation: G_4 and G_6 increase by 2.3 ± 0.1%, and the glass is closer to isotropy ($A = +0.13\%$). In this condition the glass is already substantially relaxed, because annealing at the same temperature for a further 6 days causes a further increase in G_4 and G_6 of only ~1.0%. The total increases in the shear moduli are relatively small, possibly because the 'as-cast' glass is already rather relaxed through prolonged storage at room temperature, which in this case is 0.63 T_g.

Next, the sample was subjected to creep at RT, loading in uniaxial compression at 200 MPa (0.3 σ_y) for 24 h. After this loading, the sample was stored stress-free at RT for more than 24 h to allow full anelastic recovery. Then the RUS measurements show that the glass remains isotropic, and the moduli have decreased (by 0.3–0.4%) relative to the 6-day annealed. This decrease is comparable to that found in loading of a Zr-based BMG [36], but in the present work we can verify that isotropy is maintained. The decrease in the moduli is an example of *rejuvenation* (the opposite of relaxation or ageing) and is consistent with property changes (enthalpy increase and density decrease) seen after *elastostatic* uniaxial compressive loading of BMG samples [36]. In the present work, however, the loading stress, as a fraction of σ_y, is much lower than in the previous studies. The rejuvenation is associated with the viscoplastic component of the strain, ε_v, and is attributed to dilatation induced by the shear flow during creep [37].

Lastly, this sample was subjected to creep under the same stress, but at 380 K (0.8 T_g) for 2 h. After cooling from this temperature, the sample shows moduli that are further reduced; evidently the rejuvenation effect of the shearing during creep outweighs the relaxation expected at the elevated temperature. The main result, however, is that high-temperature creep induces anisotropy ($A = -1.4\%$) that lies outside the experimental uncertainty. The negative A is consistent with that found for $Pd_{40}Cu_{30}Ni_{10}P_{20}$ BMG in the early stages of creep induced by similar loading in compression at elevated temperature (0.89–0.98 T_g) [13]. The anisotropy in this regime is attributed to frozen-in anelastic strain ε_a [13]. Thus the effects of ε_a and ε_v can be superposed.

Overall, Fig. 3 shows that RUS measurements of the complete

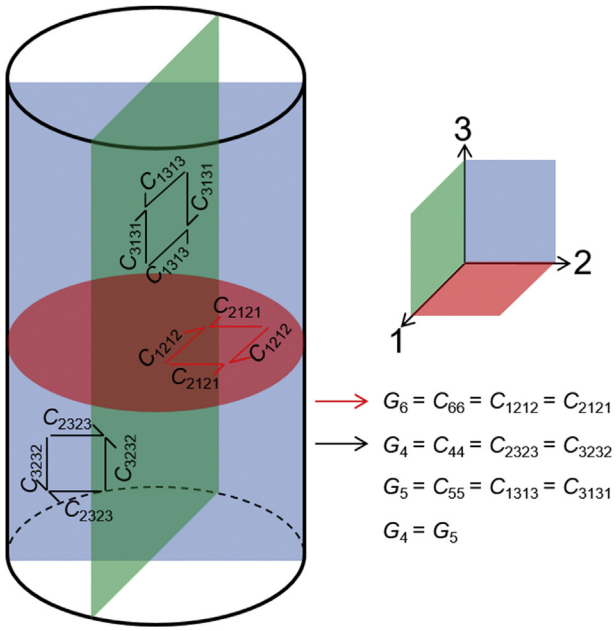

Fig. 2. Reference axes for the cylindrical samples subjected to uniaxial loading parallel to the cylinder (3) axis. The samples are expected to remain isotropic in the transverse (1,2) plane. Shear directions for stiffness coefficients C_{ijij} are shown in three orthogonal planes: the red arrows are for the modulus G_6 and the black arrows for G_4. (For interpretation of the references to colour in this figure legend, the reader is referred to the web version of this article.)

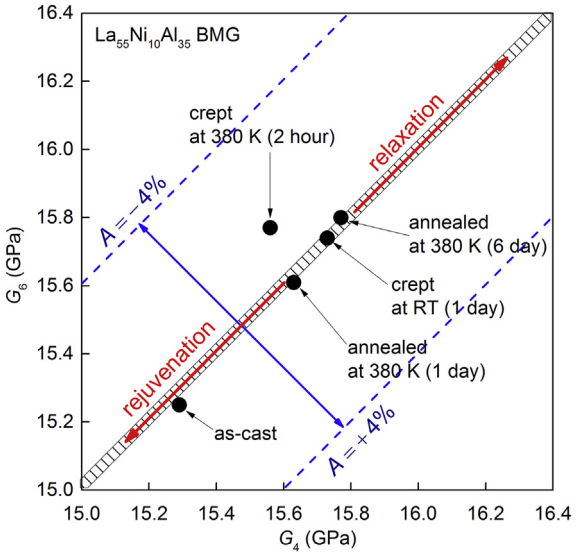

Fig. 3. Shear moduli G_4 and G_6 (Fig. 2) of a single cylindrical sample of $La_{55}Ni_{10}Al_{35}$ BMG, as-cast and after a sequence of treatments: annealing at 380 K (0.8 T_g) for 1 day, a further anneal at 380 K for 6 days, then compressive creep (at 200 MPa, 0.3 σ_y) first at RT for 1 day and finally at 380 K for 2 h. The shaded band indicates isotropy of the sample within the experimental error (±0.02 GPa in the modulus values). The red arrows indicate the directions of change for relaxation and rejuvenation of a sample that continues to be isotropic. The blue arrows indicate induced anisotropy at a given degree of relaxation. The sample crept at 380 K for 2 h shows negative anisotropy A (Eq. (1)); for compressive treatments (as confirmed for the Ce-based and Pd-based BMGs in the present work), this sign of anisotropy is associated with frozen-in anelastic strain. (For interpretation of the references to colour in this figure legend, the reader is referred to the web version of this article.)

elasticity tensor are useful for quantification of subtle deformation-induced structural changes, distinguishing induced anisotropy from relaxation and rejuvenation.

3.2. Anelastic recovery

Anelastic recovery of BMG samples has been characterized directly in real time through strain measurements. For example, for a Zr-based BMG for which RT is 0.48 T_g, the anelastic strain seems fully recovered after 4.5 h [36]. We attempt here to characterize the elastic property changes associated with anelastic recovery. A sample of $Ce_{65}Al_{10}Cu_{20}Co_5$ BMG was loaded in uniaxial compression at 285 MPa (0.5σ_y) at RT (0.8T_g for this glass) for 6 h. After unloading, RUS measurements were made at RT; the first measurement was made after a lapse of some 20 min and data collection continued up to a total of 90 min. For speed of data acquisition, the behaviour of only one resonance peak was monitored (Fig. 4a). This was the fourth lowest-frequency peak, chosen because it is well separated from its neighbours. It is 87% dependent on shear-mode vibration.

This first resonance peak shifts relatively rapidly over the first 300 s of measurement, and appears to saturate after a total time of about 50 min (Fig. 4b); at this point the resonant frequency is higher than, but within 0.2% of that of the sample before loading. Though beyond the scope of the present work, the shape of the relaxation curve in Fig. 4b, suggests the operation of discrete processes, such as have been suggested for stress relief in metallic glasses [38]. It is clear that the initial recovery is rapid; the form of the curve suggests that the total anelastic recovery corresponds to a large modulus change of at least several percent. Anelastic strain induced by loading at RT obviously cannot be preserved at RT. But if the loading is at higher temperature, some of the induced anelastic strain can be frozen in at RT. The form of the anelastic recovery seen in Fig. 4b and in Ref. [36], however, suggests that if unloading is followed by cooling to RT, a significant fraction of the induced anelastic effects may be lost due to rapid initial recovery.

The data in Fig. 4 provide the first direct evidence that anelastic strain recovery leads to measurable changes in elastic properties. Next, we contrast these changes with those induced by viscoplastic strain.

3.3. Anisotropy induced by plastic flow

For comparison with earlier work [13], $Pd_{40}Cu_{30}Ni_{10}P_{20}$ BMG was subjected to constant-strain-rate tests in uniaxial compression. Fig. 5 shows the engineering stress-strain curve for a sample loaded at 10^{-3} s^{-1} and 548 K (0.96 T_g). The elastic portion of the curve is followed by a drop in flow stress; flow causes a decrease in viscosity, associated with disordering and dilatation of the glass. In this non-Newtonian regime, steady-state flow is established, with viscosity dependent on strain rate [39]. In the present case, the steady state is not evident because the increase in sample cross-section causes the engineering stress to rise.

Similar compression tests on samples of the same BMG were stopped at different final strains. After quenching, a cuboid was cut from each deformed sample. RUS was then used to determine the stiffness coefficients in the transverse-isotropic elasticity tensor. Values of the anisotropy A (Eq. (1)) are given at the corresponding strains on Fig. 5. In agreement with previous results [13] a negative anisotropy first develops and then reverses sign. By determining the extent to which induced anisotropy was reduced by subsequent annealing, Concustell et al. [13] inferred that, under compression, negative A is associated with anelastic strain and positive A with viscoplastic strain. The data in Fig. 5 now provide direct confirmation of this by correlating the induced anisotropy with the stress-strain curve. The most negative observed A is at the onset of plastic flow, and at higher strains A evolves to more positive values.

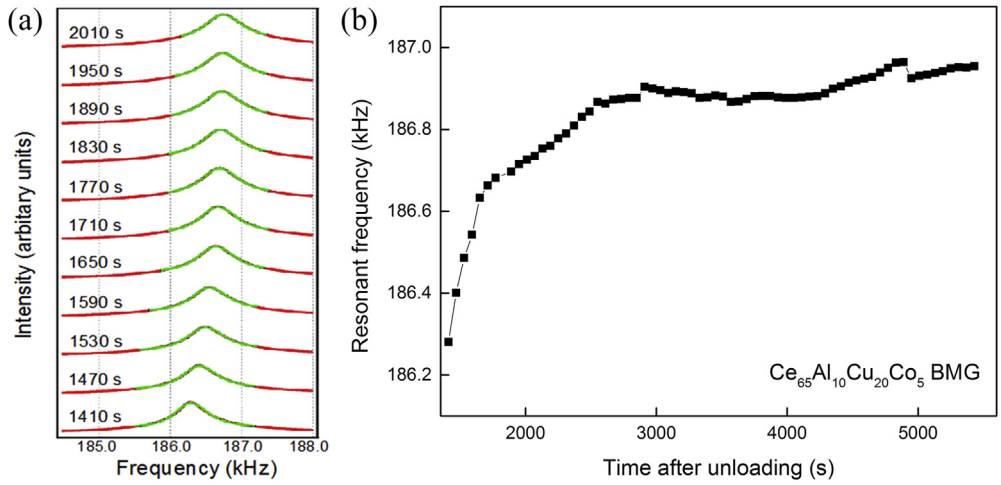

Fig. 4. Resonant ultrasound spectroscopy (RUS) characterization of an as-cast sample of $Ce_{65}Al_{10}Cu_{20}Co_5$ BMG, after loading in uniaxial compression at 285 MPa (0.5 σ_y) for 6 h at RT (0.8 T_g). The data are shown as a function of the time elapsed at RT after unloading, and reveal the anelastic recovery of the glass: (a) the selected peak in the RUS spectrum shifts to higher frequencies; (b) this shift appears to saturate after about 50 min (3000 s). The frequencies are measured to an accuracy of ±0.03 kHz.

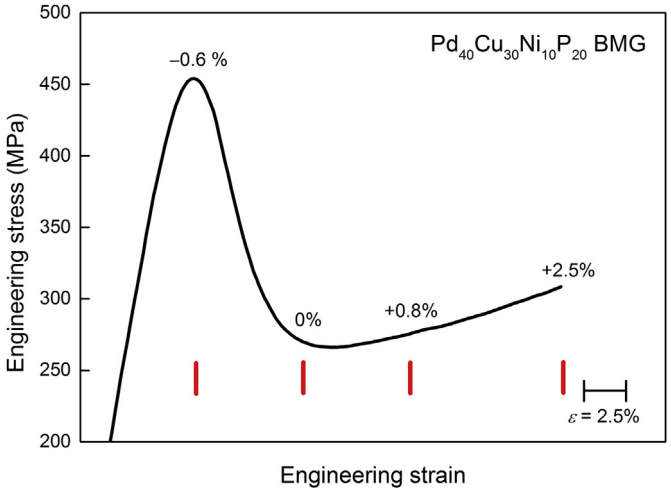

Fig. 5. The engineering stress-strain curve for an as-cast cylindrical sample of $Pd_{40}Cu_{30}Ni_{10}P_{20}$ metallic glass loaded in uniaxial compression at 548 K (0.96 T_g) and 10^{-3} s^{-1} (engineering-strain rate). Tests on separate similar samples of the same glass loaded under the same conditions were stopped at different strain values (vertical dashes); from these, cuboid samples were cut for RUS analysis. The values of anisotropy A (Eq. (1)) from these analyses are given as labels on the main curve. As-cast samples are, within experimental uncertainty, isotropic, with $|A| < 0.3\%$.

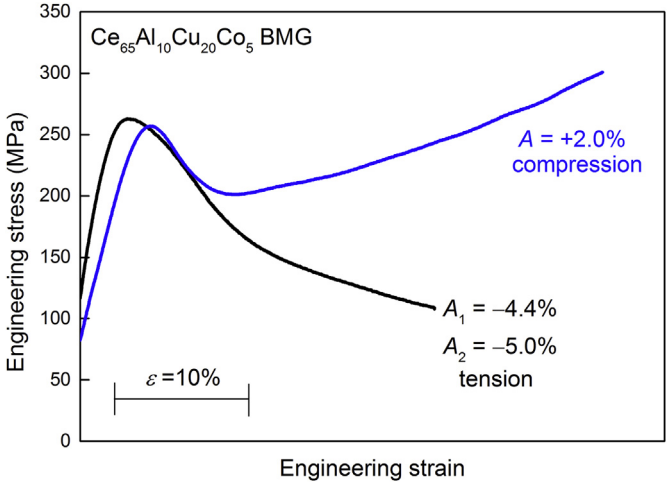

Fig. 6. Engineering stress-strain curves for as-cast cylindrical samples of $Ce_{65}Al_{10}Cu_{20}Co_5$ metallic glass loaded in uniaxial compression (at 363 K, 0.97 T_g) or in tension (at 368 K, 0.99 T_g) at 10^{-2} s^{-1} (engineering-strain rate). From the samples at the end of each test, cuboids were cut for RUS analysis, which gave values of anisotropy A (Eq. (1)) as shown.

Taking all the results on this BMG (Table 2), the maximum positive A observed for different strain rates and temperatures is 2.5% (Fig. 5), but there is no sign that this has reached a limit.

At higher temperature, the flow of BMG systems is Newtonian; there is no drop in flow stress, and the steady-state viscosity is independent of strain rate [39]. In the present work, flow at 10^{-3} s^{-1} and 569 K ($T/T_g = 1$) is presumed to be in this regime, and the resulting anisotropy at large strain (33%) is near-zero, i.e. the sample is essentially isotropic (Table 2).

3.4. Comparison of flow in tension and compression

In our previous work [13] and so far in the present work, the mechanical treatments have been in compression. We now compare the effects of constant-displacement-rate tests in compression and tension. Fig. 6 shows the engineering stress-strain curves for $Ce_{65}Al_{10}Cu_{20}Co_5$ BMG loaded at 10^{-2} s^{-1} at similar temperatures, 363 K (0.97 T_g) in compression and 368 K (0.99 T_g) in tension. The drop in flow stress is similar in both cases. At higher strains the trends in engineering stress reflect the changes in sample cross-section. In compression, as seen earlier for the Pd-based BMG (Fig. 5), the stress increases. In tension, as expected, the engineering stress falls as the sample cross-section decreases. The gauge length of the sample shows a uniform decrease in cross-section, without local necking. The plastic strain was calculated from the reduction in cross-sectional area and corresponded to a final elongation of 27 ± 3%. From the elongated gauge length, two cuboid samples were prepared for RUS, and they showed similar anisotropies of −4.4% and −5.0%. In the compression sample taken to a greater final strain (40%) the anisotropy is +2.0%.

We note that anisotropy induced by flow in compression has the same sign in both the Ce-based and Pd-based BMGs (Figs. 5 and 6). In the Ce-based BMG, and presumably in others, flow in tension and compression induce opposite signs of anisotropy. It appears that

tensile flow may induce a greater magnitude of anisotropy for a given total strain.

4. Discussion

4.1. Structural origin of induced anisotropy

As has been noted above, structural studies of induced anisotropy in MGs have focused on the effects of frozen-in anelastic strain [6,20,24]. The structural changes are considered in terms of breaking or forming interatomic bonds in the directions parallel or orthogonal to the uniaxial loading axis, and, of course, the effects are reversed in compression and tension. The effects of the frozen-in strain are detected in ellipticity of the diffraction halo, and have been widely discussed in terms of *bond orientational anisotropy* (BOA). Structural studies of this kind, when applied to MGs after deformation by viscoplastic flow, suggest that little anisotropy is induced [23]. The present results on elastic properties, corroborating those in ref. [13], show, however, that viscoplastic flow can induce significant anisotropy. The structural origins of this anisotropy now need to be explored.

For polymers, it is well known that viscoplastic elongation leads to alignment of the chains; this leads to elastic anisotropy [40,41], and can be so marked as to lead to distinct types of crystallization [42,43]. In such systems as aqueous clay suspensions when the particles can be considered as rigid discs, the hydrodynamic forces resulting from shearing induce alignment of the discs [44]. For metallic systems, however, the possible origins of flow-induced anisotropy are not so clear. The stress drops seen in stress-strain curves (Figs. 5 and 6) show clearly that flow induces structural change: in this non-Newtonian regime, higher shear rate induces greater dilatation and the steady-state viscosity is lower. This is normally considered in terms of random atomic motion inducing an isotropic change. In the present context, the key question is whether this dilatational structural change is anisotropic. Computer simulations of hard spheres [45] and direct observations of spherical-particle colloids [46] show that particle displacements are correlated, with a strong degree of anisotropy, such that the collective motion is string-like. This behaviour has also been suggested to explain length-scale effects in the relaxation of MGs [47].

In simulations of shear flow in a metallic glass, Egami et al. [20] identified well defined local configurational excitations (LCEs) involving bond cutting and creation in orientations related to the applied shear stress. The stress field created by one LCE can trigger another neighbouring LCE and ultimately lead to a cascade. Whether such non-random motion can help to explain induced anisotropy remains to be seen.

4.2. Extent of flow-induced anisotropy

Even if the mechanisms for inducing anisotropy rather than isotropic change are unknown, it is clear that structural change occurs during non-Newtonian flow, and that there must be the possibility of freezing-in this change by quenching to a lower temperature (usually RT) after flow. The extent of structural change under flow has been extensively studied in polymer rheology [48]. The degree of structural change that can be expected is related to the dimensionless Weissenberg number, Wi:

$$\mathrm{Wi} = \tau_\alpha \dot{\gamma} = \tau_\alpha / \tau_{\mathrm{shear}}, \qquad (2)$$

where τ_α is the time associated with the primary α relaxation near the glass transition, $\dot{\gamma}$ is the shear strain rate, and τ_{shear} is the shear-rate time (the inverse of the rate). The relaxation time to reach structural equilibrium after a perturbation is characterized by τ_α, and is temperature-dependent. Thus, for a given system, Wi is dependent on temperature and shear strain rate. When $\mathrm{Wi} \ll 1$, the time for structural relaxation is comparatively short, and even under flow the liquid remains in equilibrium (there is no induced structural change); when $\mathrm{Wi} \gg 1$, there is structural change. In our case, we take 'structural change' to be anisotropy, as the equilibrium liquid is isotropic.

As seen in Fig. 5, the effects of viscoplastic flow dominate over those of anelastic strain only at high-enough total strain. In plotting Fig. 7a, we select data from Table 2 with total inelastic strain ($\varepsilon_a + \varepsilon_v$) greater than 13%. The temperature (on a scale of T_g/T) and shear-rate time τ_{shear} are plotted for each of the relevant tests on the Pd- and Ce-based BMGs. Open symbols denote those test conditions leading to negligible anisotropy ($|A| < 0.3\%$), and closed symbols otherwise.

Also shown are published values of τ_α for the compositions $Pd_{40}Cu_{30}Ni_{10}P_{20}$ [49] and $Ce_{65}Al_{10}Cu_{20}Co_5$ [50]. The curves for τ_α have different slopes, reflecting the differing kinetic fragilities m (temperature dependence of the liquid viscosity at T_g, as analysed by Angell [51]). For $Pd_{40}Cu_{30}Ni_{10}P_{20}$, $m = 66$ [49]; for $Ce_{65}Al_{10}Cu_{20}Co_5$, $m = 34$ [50]. It is immediately clear from Fig. 7a that when $\tau_\alpha < \tau_{\mathrm{shear}}$ the induced anisotropy is negligible and vice versa.

The extent of induced anisotropy is shown quantitatively in Fig. 7b. This shows that significant anisotropy can be induced during flow (and can be retained on subsequent quenching) when Wi exceeds a value in the range 1–10. As Wi extends to yet higher values, the anisotropy increases, but the preliminary data do not give a clear indication of whether the anisotropies so far attained are close to saturation or not. We assume that under given flow conditions, a steady state degree of anisotropy would be attained at large strains. A probable fundamental limiting factor on the steady-state degree of anisotropy is the onset of inhomogeneous flow (i.e. *shear-banding* [21]) at higher Wi. In the present work, the practical limit was set by fracture, most likely dependent on specific defects in the samples. In smaller samples, fracture would be less likely and the onset of inhomogeneous flow would be inhibited [52]; samples with μm-scale cross-sections [52] may be best for maximizing the extent of flow-induced anisotropy.

At optimized values of Wi, viscoplastic flow can induce significant elastic anisotropy that can be substantially preserved on quenching after flow. The anisotropic samples thus produced must reveal something of the structures and mechanisms under flow. That the existing structural studies show little anisotropy in this regime suggests that ellipticity in the first diffraction halo is not a good measure of all types of anisotropy. The ellipticity shows the strain due to local anelastic deformation, but a different analysis of the diffraction data (perhaps based in real space) is needed to characterize the structural changes induced by viscoplastic flow.

5. Conclusions

This study has focused on the effects of thermomechanical treatments (constant-load, or constant-strain-rate, tests in uniaxial compression or tension) on three bulk metallic glasses (BMGs), Ce-based, La-based and Pd-based. Measurements of the full elasticity tensor using resonant ultrasound spectroscopy (RUS) provide a quantitative measure of the induced changes, and distinguish between relaxation/rejuvenation, on the one hand, and anisotropy on the other. The deformed BMGs are transverse-isotropic, and their anisotropy (which can be positive or negative) is characterized by $A = (G_4 - G_6)/G_4$, where G_4 and G_6 are shear moduli defined in a coordinate system with its 3-axis parallel to the loading axis. It is confirmed that anelastic strain, both frozen-in (as inferred in earlier work) and transient (present work), gives measurable changes in elastic properties. The sign of the induced anisotropy reverses as

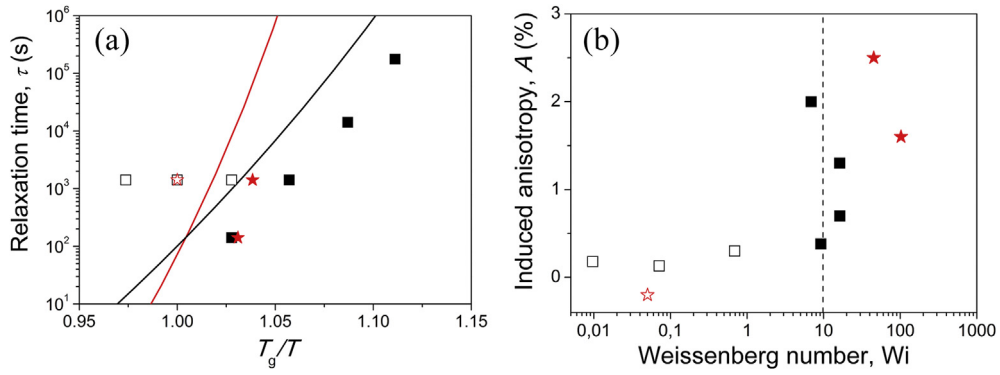

Fig. 7. Anisotropies induced by viscoplastic flow in compression in the BMGs $Pd_{40}Cu_{30}Ni_{10}P_{20}$ (red data points, stars) and $Ce_{65}Al_{10}Cu_{20}Co_5$ (black data points, squares). RUS is used to measure the elastic anisotropy of the samples after flow: open symbols denote samples with negligible anisotropy (<0.3%), and closed data points those with greater anisotropy. (a) the shear-rate times (τ_{shear}, data points, present work), compared with the structural relaxation time (τ_α, curves [49,50]). When $\tau_\alpha < \tau_{shear}$ the induced anisotropy is negligible and vice versa. (b) the magnitude of induced anisotropy as a function of the Weissenberg number Wi (Eq. (2)). Viscoplastic flow in tension (Fig. 6) gives a large anisotropy at Wi = 2.04. (For interpretation of the references to colour in this figure legend, the reader is referred to the web version of this article.)

the glass starts to flow and shows a stress drop. Under compression, the induced A is negative in the anelastic regime and positive in the flow regime; these signs are reversed if the loading is tensile. These basic phenomena (sign, and order of magnitude, of the induced anisotropy) are independent of glass composition. The degree of anisotropy induced by viscoplastic flow can exceed that due to quenched-in anelastic strain. Flow in tension appears to be more efficient in inducing anisotropy than flow in compression. The extent of anisotropy induced by viscoplastic flow can be interpreted in terms of the Weissenberg number Wi (the ratio of characteristic times for structural relaxation and for shear strain rate). For metallic glasses, we find that significant anisotropy arises for flow at Wi > (1–10). The maximum possible induced anisotropy may be obtained at higher Wi by flow as close as possible to the onset of inhomogeneous flow (shear-banding). Priorities for future study are: to characterize the structural origins of anisotropy induced by viscoplastic flow, and to exploit that characterization to better understand the mechanisms of flow and mechanical failure of metallic glasses.

Acknowledgements

This research was supported by the Engineering and the Engineering and Physical Sciences Research Council, UK (grant EP/I035404/1). Y.H.S. acknowledges support from a China Scholarship Council (CSC) scholarship. The authors thank Z. Lu, H. Y. Bai and W. H. Wang for the supply of the $Ce_{65}Al_{10}Cu_{20}Co_5$ and $La_{55}Ni_{20}Al_{25}$ metallic glasses.

All data accompanying this publication are directly available within the publication.

References

[1] H.A. Davies, J.H. Vincent, J.G. Herbertson, Comment on the paper 'Substrate-induced liquid shearing and defect anisotropy in metallic glasses' by A R Yavari and P Desré, J. Phys. F. Met. Phys. 14 (1984) 2007–2008.
[2] H.R. Sinning, L. Leonardsson, R.W. Cahn, Irreversible anisotropic length changes in $Fe_{40}Ni_{40}B_{20}$ and a search for reversible length changes in several metallic glasses, Int. J. Rapid Solid. 1 (1985) 175–197.
[3] H. Friedrichs, H. Neuhäuser, Study of structural relaxation of metallic glasses by stress-free dilatometry, J. Phys. Cond. Matter 1 (1989) 8305–8318.
[4] A.R. Yavari, P. Desré, Substrate-induced liquid shearing and defect anisotropy in metallic glasses, J. Phys. F. Met. Phys. 14 (1984) 291–299.
[5] S. Steeb, P. Lamparter, Recent structural results with amorphous alloys using neutron diffraction, J. Phys. Coll. 46 C8 (1985) 247–253.
[6] Y. Suzuki, J. Haimovich, T. Egami, Bond-orientational anisotropy in metallic glasses observed by x-ray diffraction, Phys. Rev. B 35 (1987) 2162–2168.
[7] D. Spilsbury, P. Butvin, N. Cowlam, W.S. Howells, R.J. Cooper, Some evidence for 'directional atomic pair ordering' in a cobalt-based metallic glass, Mater. Sci. Eng. A 226–228 (1997) 187–191.
[8] S. Arakawa, H. Harada, G. Hausch, H.R. Hilzinger, F.J. Menges, H. Warlimont, Anisotropy of tensile properties of amorphous metals, in: S. Steeb, H. Warlimont (Eds.), Rapidly Quenched Metals, North-Holland, Amsterdam, 1985, pp. 1389–1392.
[9] V.Z. Bengus, V. Ocelík, Structural models of the yield stress anisotropy of amorphous alloys ribbons, J. Non-Cryst. Solids 192–193 (1995) 595–598.
[10] R. Tarumi, A. Shibata, H. Ogi, M. Hirao, K. Takashima, Y. Higo, Elastic anisotropy of an $Fe_{79}Si_{12}B_9$ amorphous alloy thin film studied by ultrasound spectroscopy, J. Appl. Phys. 101 (2007) 053519.
[11] F. Hellman, Surface-induced ordering: a model for vapor-deposition growth of amorphous materials, Appl. Phys. Lett. 64 (1994) 1947–1949.
[12] S.S. Dalal, M.D. Ediger, Molecular orientation in stable glasses of indomethacin, J. Phys. Chem. Lett. 3 (2012) 1229–1233.
[13] A. Concustell, S. Godard-Desmarest, M.A. Carpenter, N. Nishiyama, A.L. Greer, Induced elastic anisotropy in a bulk metallic glass, Scr. Mater 64 (2011) 1091–1094.
[14] Y.H. Sun, A. Concustell, A.L. Greer, Thermomechanical processing of metallic glasses: extending the range of the glassy state, Nat. Rev. Mater. 1 (2016) (in press).
[15] H.F. Poulsen, J.A. Wert, J. Neuefeind, V. Honkimäki, M. Daymond, Measuring strain distributions in amorphous materials, Nat. Mater. 4 (2005) 33–36.
[16] H. Shakur Shahabi, S. Scudino, I. Kaban, M. Stoica, U. Rűtt, U. Kűhn, J. Eckert, Structural aspects of elasto-plastic deformation of a Zr-based bulk metallic glass under uniaxial compression, Acta Mater. 95 (2015) 30–36.
[17] A.L. Greer, Y.Q. Cheng, E. Ma, Shear bands in metallic glasses, Mater. Sci. Eng. R. 74 (2013) 71–132.
[18] F.O. Méar, G. Vaughan, A.R. Yavari, A.L. Greer, Residual-stress distribution in shot-peened metallic-glass plate, Philos. Mag. Lett. 88 (2008) 757–766.
[19] W. Dmowski, T. Egami, Structural anisotropy in metallic glasses induced by mechanical deformation, Adv. Eng. Mater. 10 (2008) 1003–1007.
[20] T. Egami, T. Iwashita, W. Dmowski, Mechanical properties of metallic glasses, Metals 3 (2013) 77–113.
[21] R.T. Ott, M. Heggen, M. Feuerbacher, E.S. Park, D.H. Kim, M.J. Kramer, M.F. Besser, D.J. Sordelet, Anelastic strain and structural anisotropy in homogeneously deformed $Cu_{64.5}Zr_{35.5}$ metallic glass, Acta Mater. 56 (2008) 5575–5583.
[22] M.J. Kramer, R.T. Ott, D.J. Sordelet, Anisotropic atomic structure in a homogeneously deformed metallic glass, J. Mater. Res. 22 (2007) 382–388.
[23] R.T. Ott, M.J. Kramer, M.F. Besser, D.J. Sordelet, High-energy X-ray measurements of structural anisotropy and excess free volume in a homogenously deformed Zr-based metallic glass, Acta Mater. 54 (2006) 2463–2471.
[24] W. Dmowski, Y. Tong, T. Iwashita, Y. Yokoyama, T. Egami, Universal mechanism of thermomechanical deformation in metallic glasses, Phys. Rev. B 91 (2015), 060101(R).
[25] O.V. Nielsen, H.J.V. Nielsen, Magnetic anisotropy in $Co_{73}Mo_2Si_{15}B_{10}$ and $(Co_{0.89}Fe_{0.11})_{72}Mo_3Si_{15}B_{10}$ metallic glasses, induced by stress-annealing, J. Magn. Magn. Mater. 22 (1980) 21–24.
[26] O.V. Nielsen, A. Hernando, V. Madurga, J.M. Gonzalez, Experiments concerning the origin of stress anneal induced magnetic anisotropy in metallic glass ribbons, J. Magn. Magn. Mater. 46 (1985) 341–349.
[27] M.L. Fernández-Gubieda, J.M. Barandiarán, O.V. Nielsen, Simultaneous observation of viscoelastic deformation and induced magnetic anisotropy in $[Co_{1-x}(FeNi)_x]_{75}Si_{15}B_{10}$ metallic glasses, J. Appl. Phys. 62 (1987) 2579–2582.
[28] L. Kraus, G. Vlasák, Creep-induced magnetic anisotropy and anelastic strain of an iron-rich amorphous alloy, Mater. Sci. Eng. B 15 (1992) 121–125.
[29] L. Kraus, M. Vázquez, A. Hernando, Creep-induced magnetic anisotropy in a

Co-rich amorphous wire, J. Appl. Phys. 76 (1994) 5343–5348.
[30] J. Qiang, D. Estevez, Y. Dong, Q. Man, C. Chang, X. Wang, R.W. Li, Giant magnetoimpedance effect enhanced by thermoplastic drawing, J. Appl. Phys. 116 (2014) 093911.
[31] Y. Tong, W. Dmowski, Y. Yokoyama, G. Wang, P.K. Liaw, T. Egami, Recovering compressive plasticity of bulk metallic glasses by high-temperature creep, Scr. Mater. 69 (2013) 570–573.
[32] R.E.A. McKnight, M.A. Carpenter, T.W. Darling, A. Buckley, P.A. Taylor, Acoustic dissipation associated with phase transitions in lawsonite, $CaAl_2Si_2O_7(OH)_2 \cdot H_2O$, Am. Mineral. 92 (2007) 1665–1672.
[33] R.E.A. McKnight, T. Moxon, A. Buckley, P.A. Taylor, T.W. Darling, M.A. Carpenter, Grain size dependence of elastic anomalies accompanying the $\alpha-\beta$ phase transition in polycrystalline quartz, J. Phys. Condens. Matter 20 (2008) 075229.
[34] A. Migliori, J.L. Sarrao, Resonant Ultrasound Spectroscopy: Applications to Physics, Material Measurements and Nondestructive Evaluation, Wiley, New York, 1997.
[35] G. Kaplan, T.W. Darling, K.R. McCall, Resonant ultrasound spectroscopy and homogeneity in polycrystals, Ultrasonics 49 (2009) 139–142.
[36] H.B. Ke, P. Wen, H.L. Peng, W.H. Wang, A.L. Greer, Scr. Mater. 64 (2011) 966–969.
[37] Y.H. Sun, A.L. Greer, Stored energy in metallic glasses due to elastic and thermal strains, Philos. Mag. (2016) (in press).
[38] J.D. Ju, D. Jang, A. Nwankpa, M. Atzmon, An atomically quantized hierarchy of shear transformation zones in a metallic glass, J. Appl. Phys. 109 (2011) 053522.
[39] J. Lu, G. Ravichandran, W.L. Johnson, Deformation behavior of the $Zr_{41.2}Ti_{13.8}Cu_{12.5}Ni_{10}Be_{22.5}$ bulk metallic glass over a wide range of strain-rates and temperatures, Acta Mater. 51 (2003) 3429–3443.
[40] M. Negahban, A. Goel, L.L. Zhang, Evaluating the development of elastic anisotropy with plastic flow, Acta Mech. 208 (2009) 259–267.
[41] X.J. Wang, V. Ho, R.A. Segalman, D.G. Cahill, Thermal conductivity of high-modulus polymer fibers, Macromolecules 46 (2013) 4937–4943.
[42] A.J. Pennings, J.M.A.A. van der Mark, A.M. Kiel, Hydrodynamically induced crystallization of polymers from solution: III. Morphology, Kolloid Z. Z. Polym. 237 (1970) 336–358.
[43] I. Dukovski, M. Muthukumar, Langevin dynamics simulations of early stage shish-kebab crystallization of polymers in extensional flow, J. Chem. Phys. 118 (2003) 6648–6655.
[44] C. Baravian, D. Vantelon, F. Thomas, Rheological determination of interaction potential energy for aqueous clay suspensions, Langmuir 19 (2003) 8109–8114.
[45] B. Doliwa, A. Heuer, Cooperativity and spatial correlations near the glass transition: computer simulation results for hard spheres and disks, Phys. Rev. E 61 (2000) 6898–6908.
[46] E.R. Weeks, D.A. Weitz, Properties of cage rearrangements observed near the colloidal glass transition, Phys. Rev. Lett. 89 (2002) 095704.
[47] D. Bedorf, K. Samwer, Length scale effects on relaxations in metallic glasses, J. Non-Cryst. Solids 356 (2010) 340–343.
[48] J.M. Dealy, J. Wang, Melt Rheology and its Applications in the Plastic Industry, second ed., Springer, Dordrecht, 2013.
[49] J. Qiao, R. Casalini, J.M. Pelletier, H. Kato, Characteristics of the structural and Johari–Goldstein relaxations in Pd-based metallic glass-forming liquids, J. Phys. Chem. B 118 (2014) 3720–3730.
[50] T. Wang, Y.Q. Yang, J.B. Li, G.H. Rao, Thermodynamics and structural relaxation in Ce-based bulk metallic glass-forming liquids, J. Alloys Comp. 509 (2011) 4569–4573.
[51] C.A. Angell, Formation of glasses from liquids and biopolymers, Science 267 (1995) 1924–1935.
[52] L. Tian, Y.-Q. Cheng, Z.-W. Shan, J. Li, C.-C. Wang, X.-D. Han, J. Sun, E. Ma, Approaching the ideal elastic limit of metallic glasses, Nat. Comm. 3 (2012) 609.